doi:10.1093/jmcb/mjab062
Published online October 5, 2021

Article

α1A and α1C form microtubules to display distinct properties mainly mediated by their C-terminal tails

Lei Diao[1], Ming-Yi Liu[1,2], Yin-Long Song[3], Xu Zhang[2,4], Xin Liang[3,*], and Lan Bao[1,2,*]

[1] State Key Laboratory of Cell Biology, Shanghai Institute of Biochemistry and Cell Biology, Center for Excellence in Molecular Cell Science, University of Chinese Academy of Sciences, Chinese Academy of Sciences, Shanghai 200031, China
[2] School of Life Science and Technology, ShanghaiTech University, Shanghai 201210, China
[3] Tsinghua-Peking Joint Center for Life Sciences, School of Life Sciences, Tsinghua University, Beijing 100084, China
[4] Shanghai Advanced Research Institute, Chinese Academy of Sciences, Shanghai 201210, China
* Correspondence to: Lan Bao, E-mail: baolan@sibcb.ac.cn; Xin Liang, E-mail: xinliang@tsinghua.edu.cn

Edited by Xuebiao Yao

Microtubules consisting of α/β-tubulin dimers play critical roles in cells. More than seven genes encode α-tubulin in vertebrates. However, the property of microtubules composed of different α-tubulin isotypes is largely unknown. Here, we purified recombinant tubulin heterodimers of mouse α-tubulin isotypes including α1A and α1C with β-tubulin isotype β2A. *In vitro* microtubule reconstitution assay detected that α1C/β2A microtubules grew faster and underwent catastrophe less frequently than α1A/β2A microtubules. Generation of chimeric tail-swapped and point-mutation tubulins revealed that the carboxyl-terminal (C-terminal) tails of α-tubulin isotypes largely accounted for the differences in polymerization dynamics of α1A/β2A and α1C/β2A microtubules. Kinetics analysis showed that in comparison to α1A/β2A microtubules, α1C/β2A microtubules displayed higher on-rate, lower off-rate, and similar GTP hydrolysis rate at the plus-end, suggesting a contribution of higher plus-end affinity to faster growth and less frequent catastrophe of α1C/β2A microtubules. Furthermore, EB1 had a higher binding ability to α1C/β2A microtubules than to α1A/β2A ones, which could also be attributed to the difference in the C-terminal tails of these two α-tubulin isotypes. Thus, α-tubulin isotypes diversify microtubule properties, which, to a great extent, could be accounted by their C-terminal tails.

Keywords: α-tubulin isotype, microtubule dynamics, TIRF

Introduction

Microtubules consisting of α/β-tubulin heterodimers have diverse and critical roles in eukaryotic cellular processes including intracellular transport, cell migration, and cell division (Heald and Khodjakov, 2015; ChakraborTi et al., 2016). They are highly dynamic tubular polymers that stochastically switch between growing and shrinking phases, termed dynamic instability (Mitchison and Kirschner, 1984), which is important for their versatile cellular functions. Eukaryotes have multiple tubulin genes. For example, budding yeast has two α-tubulin and one β-tubulin genes (Neff et al., 1983; Schatz et al., 1986), *Drosophila melanogaster* encodes four α-tubulin and four β-tubulin isotypes (Theurkauf et al., 1986; Fackenthal et al., 1993), and mouse has at least seven α-tubulin and eight β-tubulin genes (Breuss and Keays, 2014). Each tubulin gene encodes a specific isotype that displays a unique expression profile in cells or tissues. Tubulin β3 is specifically expressed in neurons and regarded as a classic neuronal marker (Jiang and Oblinger, 1992), β2A/B is enriched in brain and epithelial cells, and β1 is mainly expressed in platelets and hematopoietic cells (Banerjee et al., 1988; Lecine et al., 2000). Furthermore, *in vivo* studies have shown that some specific tubulin isotypes are not functionally interchangeable. In mice, embryonic knockdown of the expression of neuronal tubulin β3 led to neural migration defects that could not be rescued by expression of β1, β2B, or β4A (Saillour et al., 2014). In *D. melanogaster*, when the testes-specific tubulin β2 was replaced with β3 in the male germ line, axoneme assembly and other microtubule-mediated processes including

Received June 26, 2021. Revised August 25, 2021. Accepted August 26, 2021.

meiosis and nuclear shaping were no longer occurred (Hoyle and Raff, 1990). These studies combine to indicate that microtubules consisted of different tubulin isotypes display distinct properties.

Previous studies have reported that some tubulin isotypes affect microtubule dynamics. The results from purified α/β2, α/β3, and α/β4 isotypes in bovine brain by immuno-affinity chromatography showed that microtubules made from α/β3 were more dynamic than those composed from α/β2, α/β4, or unfractionated phosphocellulose-purified brain tubulin (Panda et al., 1994). A recent study from purified recombinant tubulin isotype using a baculovirus expression system of insect cells found that the catastrophe frequency of α/β3 microtubules was higher than that of α/β2B ones (Pamula et al., 2016). Another study showed that recombinant α1A/β3 microtubules were polymerized more slowly and had fewer catastrophes than brain microtubules (Vemu et al., 2016). Tubulin purified from human embryonic kidney cells (tsA 201) predominantly consists of one α-tubulin isotype α1B and two β-tubulin isotypes, β1 and β4B. *In vitro* microtubule reconstitution assay showed that these microtubules grew faster and underwent catastrophe less frequently than brain microtubules (Vemu et al., 2017). Furthermore, recent work also revealed that the structured core of human β-tubulin was crucial for establishing isotype-specific parameters of microtubule dynamic instability (Pamula et al., 2016). Therefore, microtubules assembled with different β-tubulin isotypes have distinct polymerization properties.

Both α-tubulin and β-tubulin isotypes are highly conserved, especially the ~400-amino acid core structure of tubulin, 97% and 95% identities existed among the core structure of α-tubulin and β-tubulin in the vertebrate, respectively (Sirajuddin et al., 2014). In contrast, the unstructured carboxyl-terminal (C-terminal) tails of tubulins are the most variable part among both α-tubulin and β-tubulin isotypes. Compared to β-tubulin, α-tubulin isotypes are much less divergent. However, little is known so far about the specific functions of α-tubulin isotypes on microtubule dynamics. Previous studies report that tubulin α1A is highly expressed in post-mitotic neurons, in the human and mouse brain (Bamji and Miller, 1996; Gloster et al., 1999). Notably, *TUBA1A* is the first reported tubulin gene with >60 mutations associated with human brain malformation (Keays et al., 2007; Bahi-Buisson et al., 2014). Recently, another tubulin α1 family member, α1C, is revealed to be implicated in cell proliferation and cell cycle of various tumors (Wang et al., 2017; Albahde et al., 2020; Bian et al., 2021). Considering the important functions of tubulin α1 family members, we purified mouse recombinant tubulin heterodimers composed of tubulin α1 family members including α1A, α1B, and α1C with β2A, a broadly expressed isotype of β-tubulin, and detected the differences in the dynamics of microtubules composed of three different α-tubulin isotypes. Compared with α1A/β2A microtubules, α1C/β2A microtubules grew faster and had a lower catastrophe frequency. Further experiments with the chimeric tail-swapped and point-mutation tubulins showed that the different C-terminal tails of α1A and α1C accounted for the different polymerization dynamics at microtubule plus-ends. Kinetics analysis revealed that α1C/β2A had a higher affinity for the growing microtubule plus-ends than α1A/β2A. In addition, EB1 showed a higher binding ability to α1C/β2A microtubules than α1A/β2A ones, while the motility of kinesin-1 was similar for both types of microtubules, demonstrating different effects of various α-tubulin isotypes on the interaction between microtubules and different microtubule-associated proteins (MAPs). In all, our study not only reveals a significant effect of different α-tubulin isotype composition on microtubule dynamics but also provides evidence for the important roles of α-tubulin isotypes in the 'tubulin code' theory.

Results

Microtubules composed of mouse α-tubulin isotype α1A, α1B, or α1C display different dynamics

The amino acid sequences of α1A, α1B, and α1C are highly conserved. α1A only has two and eight different amino acids with α1B and α1C, respectively (Supplementary Figure S1A). To determine the polymerization properties of these α-tubulin isotypes, we expressed and purified α1A/β2A, α1B/β2A, and α1C/β2A tubulin heterodimers from insect cells using a protocol modified from the previously published methods (Minoura et al., 2013; Vemu et al., 2016; Ti et al., 2020). Homogeneous and single-isotype mouse α/β-tubulins were purified through a double-selection strategy using His-tagged α-tubulin isotypes (α1A, α1B, and α1C) and a Flag-tagged β-tubulin isotype (β2A) (Figure 1A). We typically yielded >90% pure mouse tubulin dimers from cultured insect cells, which were then used for further biochemical and biophysical analyses (Figure 1B; Supplementary Figure S1B). In the presence of microtubule seeds, mouse α1A/β2A, α1B/β2A, or α1C/β2A was able to polymerize into microtubules, respectively, which were visualized by mixing 4% HiLyte-488-labeled brain tubulin (Figure 1C). Moreover, the images from cryo-electron microscopy (Cryo-EM) showed that both α1A/β2A and α1C/β2A could form microtubules without mixed brain tubulin and microtubule seeds in the presence of GMPCPP, a slowly hydrolyzable analog of GTP (Figure 1D), supporting the capability of microtubule polymerization with single α/β-tubulin isotype. Thus, single mouse α-tubulin isotype with a β-tubulin isotype is able to be successfully purified and form microtubules.

To examine the dynamics of α1A/β2A, α1B/β2A, and α1C/β2A microtubules, we performed *in vitro* microtubule reconstitution assay using total internal reflection fluorescent (TIRF) microscopy (Figure 1E). In the presence of mouse microtubule seeds, 7.5 μM purified soluble tubulin containing 4% HiLyte-488-labeled brain tubulin was applied to observe the dynamics of microtubule polymerization. To quantify the parameters of microtubule dynamics, we generated kymographs from time-lapse images (Figure 1F). The plus-end growth rate of α1C/β2A microtubules was ~2-fold as fast as that of α1A/β2A and α1B/β2A microtubules (Figure 1G). The catastrophe frequency of α1A/β2A and α1B/β2A microtubules was similar, while the

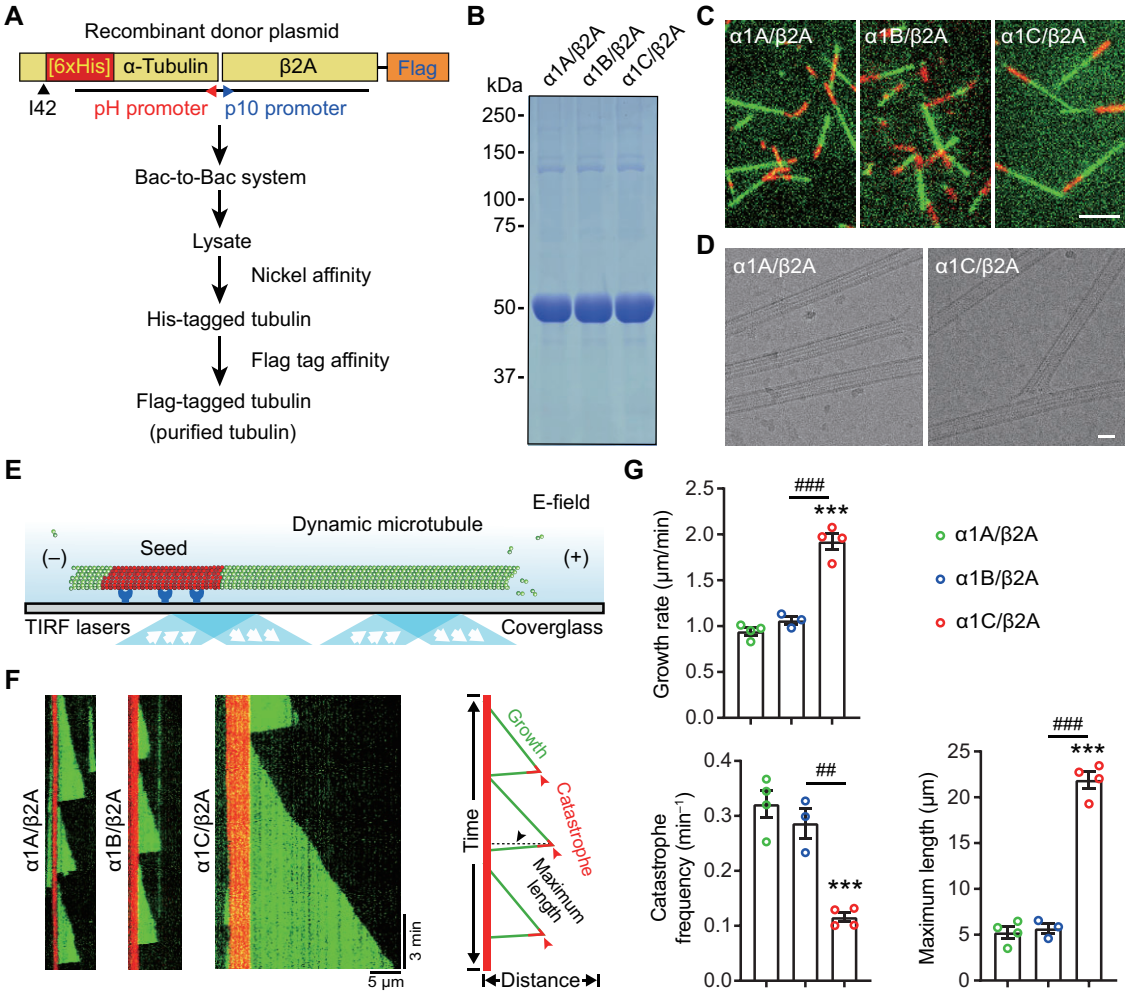

Figure 1 Dynamics of α1A/β2A, α1B/β2A, and α1C/β2A microtubules. (**A**) Schematic for purification of recombinant tubulin isotypes. (**B**) Coomassie blue staining of purified α1A/β2A, α1B/β2A, and α1C/β2A. (**C**) TIRF images of microtubules formed by α1A/β2A, α1B/β2A, or α1C/β2A in the presence of GMPCPP-stabilized microtubule seeds (red). HiLyte-488-labeled porcine brain tubulin (~4%) was added to visualize microtubules (green). Scale bar, 5 μm. (**D**) Cryo-EM images of microtubules formed by α1A/β2A and α1C/β2A, respectively, in the presence of GMPCPP. Scale bar, 25 nm. (**E**) Schematic for *in vitro* microtubule reconstitution assay used to analyze microtubule dynamics. (**F**) Kymographs showing typical microtubule growth of 7.5 μM α1A/β2A, α1B/β2A, and α1C/β2A, respectively. (**G**) Histograms showing the growth rate, catastrophe frequency, and maximum length of α1A/β2A ($n = 4$, containing 157 microtubules), α1B/β2A ($n = 3$, containing 221 microtubules), and α1C/β2A microtubules ($n = 4$, containing 87 microtubules) at the plus-end. The data are presented as mean ± SEM. $^{***}P < 0.001$ vs. α1A/β2A microtubules and $^{\#\#}P < 0.01$, $^{\#\#\#}P < 0.001$ vs. indicated; Student's *t*-test.

catastrophe frequency of α1C/β2A microtubules was one-third as low as that of α1A/β2A and α1B/β2A microtubules (Figure 1G). We further calculated the maximum microtubule length during its growth episode. The maximum length of α1A/β2A and α1B/β2A microtubules was similar, while the maximum length of α1C/β2A microtubules was significantly longer than that of α1A/β2A and α1B/β2A microtubules (Figure 1G). Because microtubule polymerization was rarely observed at minus ends at 7.5 μM tubulin, the polymerization property of microtubule at minus ends was not quantified. Taken together, these data suggest that the polymerization dynamics of microtubules composed of α1A/β2A, α1B/β2A, or α1C/β2A is largely diverse, in which α1C/β2A microtubules grow more rapidly and have a lower catastrophe frequency than α1A/β2A and α1B/β2A microtubules.

The dynamics of microtubules polymerized from α1A/β2A and α1C/β2A mixture is differentially contributed by each tubulin isotype

Microtubule in cells is usually made of a mixture of multiple α-tubulin and β-tubulin isotypes. Since α1A/β2A microtubules exhibited similar dynamics with α1B/β2A ones but different from α1C/β2A ones, we mixed α1A/β2A and α1C/β2A to measure the dynamic parameters of the mixed microtubules.

In vitro microtubule reconstitution assay showed that the microtubule dynamics was tuned by the ratio of α1A/β2A to α1C/β2A (Figure 2A and B). An increased ratio of α1A/β2A to α1C/β2A at 7.5 μM tubulin reduced the growth rate and maximum length whereas boosted the catastrophe frequency of these mixed microtubules (Figure 2A and B). Meanwhile, an increased ratio of α1C/β2A to α1A/β2A at 7.5 μM tubulin increased the growth rate and maximum length but reduced the catastrophe frequency of those mixed microtubules (Figure 2A and B). However, the dynamic parameters of mixed microtubules at equal amount of α1A/β2A and α1C/β2A at 7.5 μM tubulin were not exactly in the middle between those of α1A/β2A and α1C/β2A microtubules. The growth rate and maximum length of the mixed microtubules were closer to that of α1A/β2A ones but the catastrophe frequency was prone to α1C/β2A ones (Figure 2B), providing two possibilities that the incorporation efficiency of two α-tubulin isotypes into microtubules may be unequivalent and some properties are more like to be influenced by specific tubulin isotypes. These data suggest that the dynamics of microtubules polymerized from mixed tubulins depends on the differential contribution of each tubulin isotype.

The different dynamics of α1A/β2A and α1C/β2A microtubules are largely attributed to their C-terminal tails

To explore the molecular basis of α1A and α1C to control isotype-specific polymerization property, we compared the amino acid sequences of α1A and α1C. The sequence alignment showed that α1A and α1C had eight differential amino acids, of which two located within the core structure and six resided at the C-terminal tail (Figure 3A; Supplementary Figure S1). Due to the larger difference in C-terminal tail, we first generated chimeric α-tubulin constructs with the swapped C-terminal tail between α1A and α1C, and then purified the corresponding tubulin dimers (Figure 3A; Supplementary Figure S2A). *In vitro* microtubule reconstitution assay showed that the plus-end growth rate, catastrophe frequency, and maximum length for microtubules composed of α1A swapped the C-terminal tail with α1C, α1A(α1C)/β2A, were close to the microtubules composed of α1C/β2A, while those parameters for microtubules composed of α1C swapped the C-terminal tail with α1A, α1C(α1A)/β2A, were close to the microtubules composed of α1A/β2A, at 7.5 μM tubulin (Figure 3B and C). Thus, the C-terminal tail of α-tubulin largely contributes to the differential dynamics of α1A/β2A and α1C/β2A microtubules.

A previous study reported that the structured core of human β-tubulin confers isotype-specific polymerization property (Pamula et al., 2016). We further generated α1A and α1C mutant constructs by exchanging two different amino acids within the core between α1A and α1C, and then purified corresponding proteins to dissect their effects on the dynamics of isotype-specific microtubules (Figure 3A; Supplementary Figure S2A). *In vitro* microtubule reconstitution assay showed that, at 7.5 μM tubulin, the plus-end growth rate for α1A mutants including α1A(G232S)/β2A and α1A(S287T)/β2A was similar to that of α1A/β2A microtubules, as well as the maximum length. We also noted that the catastrophe frequency of α1A(G232S)/β2A and α1A(S287T)/β2A displayed mild changes in comparison with that of α1A/β2A microtubules but were still significantly higher than that of α1C/β2A microtubules, suggesting that these two amino acids unlikely make a significant contribution in determining the catastrophe frequency (Figure 3B and C). Furthermore, although the catastrophe frequency of α1C(S232G)/β2A and α1C(T287S)/β2A microtubules remained close to that of α1C/β2A ones, the plus-end growth rate and maximum length of α1C(S232G)/β2A microtubules were similar to that of α1A/β2A microtubules (Figure 3B and C). Taken together, these data suggest that the C-terminal tails of α1A and α1C are crucial for establishing microtubule dynamics, while two differential amino acids within the core of α1A and α1C also affect some parameters of microtubule dynamics.

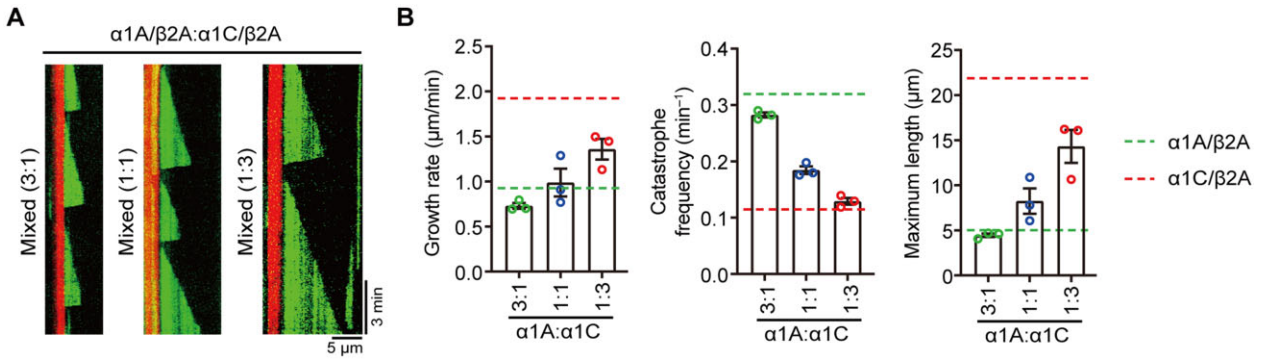

Figure 2 Dynamics of α1A/β2A and α1C/β2A mixed microtubules. (**A**) Kymographs showing typical microtubule growth of mixed 7.5 μM α1A/β2A and α1C/β2A at the ratio of 3:1, 1:1, and 1:3, respectively. (**B**) Histograms showing the growth rate, catastrophe frequency, and maximum length of microtubules mixed by α1A/β2A and α1C/β2A at the ratio of 3:1 ($n = 3$, containing 243 microtubules), 1:1 ($n = 3$, containing 211 microtubules), and 1:3 ($n = 3$, containing 218 microtubules), respectively. Growth rate, catastrophe frequency, and maximum length of α1A/β2A (green dashed line) and α1C/β2A (red dashed line) microtubules are shown for reference. The data are presented as mean ± SEM.

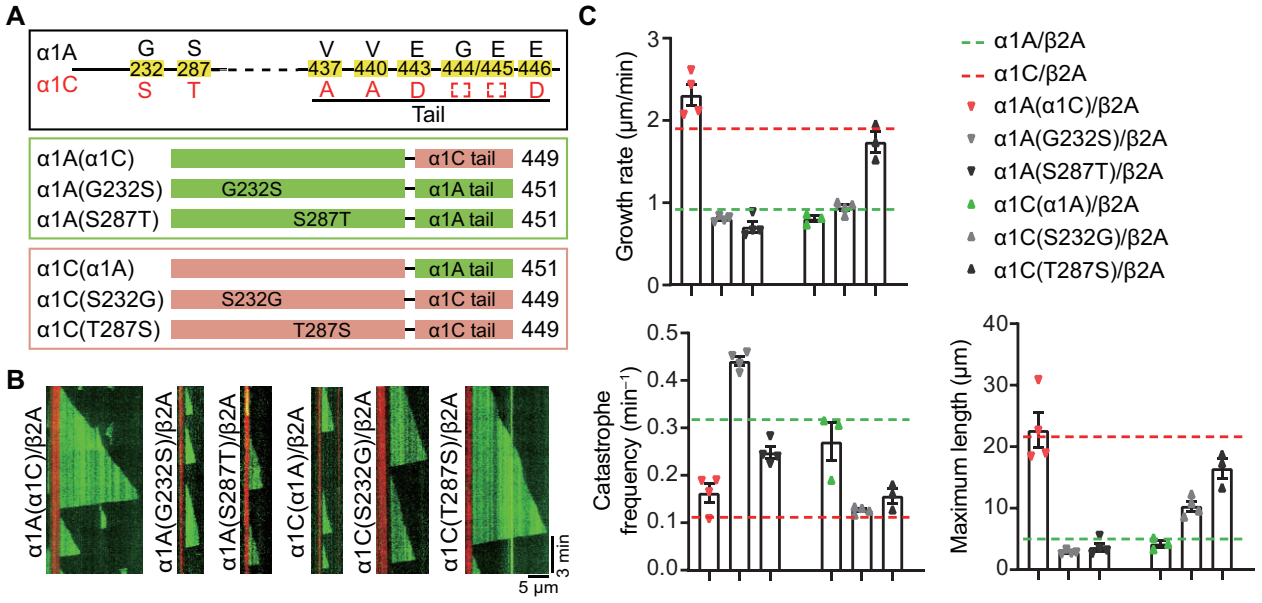

Figure 3 Dynamics of α1A(α1C)/β2A, α1C(α1A)/β2A, α1A mutant/β2A, and α1C mutant/β2A microtubules. (**A**) Sequence alignment of mouse α1A and α1C, as well as scheme of the chimeric and α-tubulin mutant constructs. (**B**) Kymographs showing typical microtubule growth of α1A(α1C)/β2A, α1C(α1A)/β2A, α1A mutant/β2A, and α1C mutant/β2A at 7.5 μM. (**C**) Histograms showing the growth rate, catastrophe frequency, and maximum length of α1A(α1C)/β2A ($n = 3$, containing 79 microtubules), α1A(G232S)/β2A ($n = 4$, containing 121 microtubules), α1A(S287T)/β2A ($n = 9$, containing 293 microtubules), α1C(α1A)/β2A ($n = 3$, containing 117 microtubules), α1C(S232G)/β2A ($n = 4$, containing 292 microtubules), and α1A(T287S)/β2A ($n = 3$, containing 90 microtubules) microtubules at the plus-end. Growth rate, catastrophe frequency, and maximum length of α1A/β2A (green dashed line) and α1C/β2A (red dashed line) microtubules are shown for reference. The data are presented as mean ± SEM.

α1C/β2A has a higher affinity for microtubule plus-ends than α1A/β2A

To understand the biochemical mechanisms underlying the different polymerization dynamics of α1A/β2A and α1C/β2A microtubules, we measured the growth rate of microtubules at various tubulin concentrations and fitted the data to the following formula:

$$r_{\text{growth}} = k_{\text{on}} \cdot [\text{Tub}] - k_{\text{off}},$$

where r_{growth} is the growth rate of microtubules and [Tub] is the concentration of tubulin dimers to calculate the apparent on-rate (k_{on}) and off-rate (k_{off}) of the polymerization dynamics (Oosawa, 1970; Pamula et al., 2016). The k_{on} of α1C/β2A was significantly higher than that of α1A/β2A, while the k_{off} of α1C/β2A was significantly lower than that of α1A/β2A (Figure 4A and Table 1). Surprisingly, we found that α1C/β2A microtubules nucleated from the templates at tubulin concentration as low as 2.5 μM, while with a similar growth rate, α1A/β2A microtubules required 5 μM tubulin (Figure 4A). The nucleation threshold of α1C/β2A is lower than that of reported α/β2B, α/β3, α1B/(β1 + β4B), α1A/β3, and brain tubulin at ~6 μM (Pamula et al., 2016; Vemu et al., 2017), indicating that α1C/β2A has a strong ability to polymerize. In all, these results provide an explanation for the higher growth rate of α1C/β2A in comparison to α1A/β2A.

We further performed this analysis on α1A(α1C)/β2A, α1C(α1A)/β2A, α1A mutant/β2A, and α1C mutant/β2A. We found that the microtubule polymerization dynamics was reversed when α1A and α1C exchanged their C-terminal tails, while the microtubule polymerization dynamics of mutants, excepted for α1C(S232G)/β2A, was similar to that of their original tubulin isotypes (Figure 4B–D and Table 1). The k_{on} of α1C(S232G)/β2A was greater than that of α1A/β2A; however, the k_{off} of α1C(S232G)/β2A was the largest among those tested tubulin isotypes and mutants (Figure 4D and Table 1), which maybe the reason why α1C(S232G)/β2A microtubules had a slower growth rate and finally caused a shorter maximum length at the plus-ends (Figure 3B and C). These results suggest that the C-terminal tails of α1A and α1C are important in determining growth rates of microtubules, and the S232 in α1C also contributes to microtubule assembly dynamics.

α1A/β2A and α1C/β2A microtubules exhibit similar GTP hydrolysis rates

We then explored the mechanism underlying the different catastrophe frequencies of α1A/β2A and α1C/β2A microtubules. Based on the GTP-cap model, the stabilizing cap at the growing ends of microtubules protects the dynamic microtubules from catastrophe. Larger stabilizing cap confers greater stability to microtubules and thereby leads to a lower catastrophe frequency (Duellberg et al., 2016). The size of stabilizing cap is determined by two factors, namely that a faster growth rate

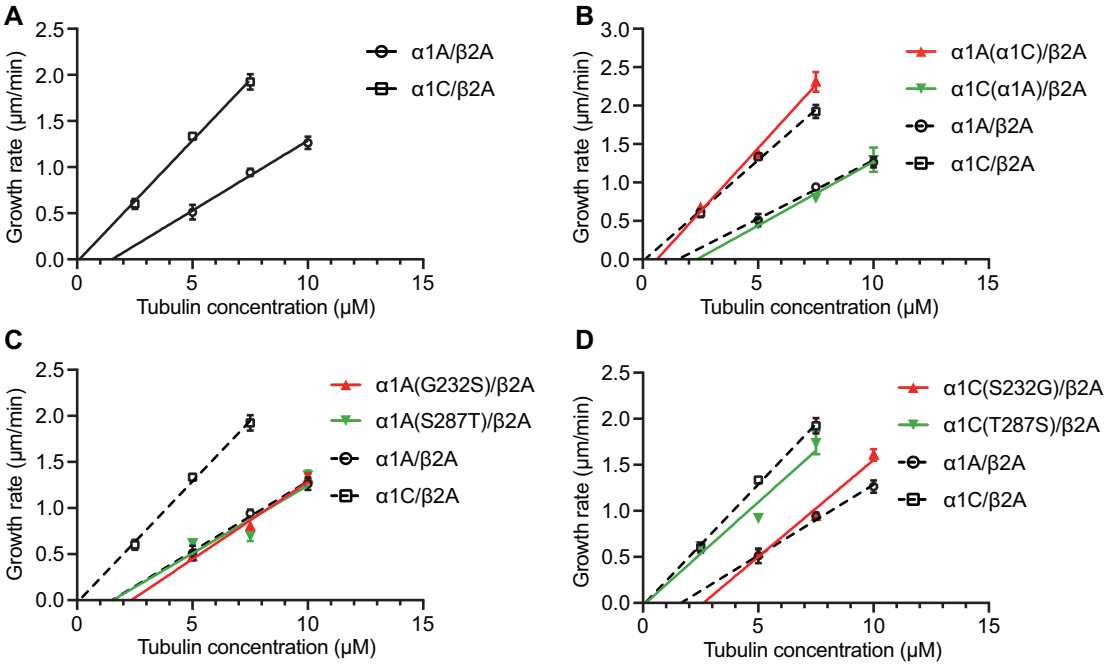

Figure 4 α1A/β2A and α1C/β2A microtubules display distinct polymerization dynamics. The mean growth rates of microtubules at different tubulin concentrations were fitted by a linear regression ($n = 3–9$, containing 39–295 microtubules) for α1A/β2A and α1C/β2A (**A**), α1A(α1C)/β2A and α1C(α1A)/β2A (**B**), α1A(G232S)/β2A and α1A(S287T)/β2A (**C**), and α1C(S232G)/β2A and α1C(T287S)/β2A (**D**) microtubules. The data are presented as mean ± SD.

Table 1 The rate constants for recombinant tubulin dimers.

Recombinant tubulin dimers	k_{on} [dimers/(μM sec)]	k_{off} (dimers/sec)
α1A/β2A	4.0 ± 0.4	4.8 ± 3.6
α1A(α1C)/β2A	8.0 ± 0.6	2.5 ± 2.4
α1A(G232S)/β2A	4.4 ± 0.4	9.3 ± 2.5
α1A(S287T)/β2A	4.0 ± 0.2	3.0 ± 1.3
α1C/β2A	7.2 ± 0.2	1.7 ± 1.1
α1C(α1A)/β2A	3.9 ± 0.4	7.0 ± 2.7
α1C(S232G)/β2A	5.5 ± 0.9	14.1 ± 6.8
α1C(T287S)/β2A	6.8 ± 0.1	3.4 ± 0.4

Measurements are from the data presented in Figure 4. The data are presented as mean ± SD.

increases the cap size and a higher GTP hydrolysis rate reduces the cap size (Bowne-Anderson et al., 2013). Obviously, the faster growth rate of α1C/β2A could lead to the smaller catastrophe frequency. To further address whether the potential change in GTP hydrolysis rate was involved in this process, we performed a TIRF-based single-molecule assay to measure the length of EB1 comets, a readout of the maturation rate of stabilizing caps, at the growing ends of microtubules (Figure 5A; Supplementary Figure S2B; Maurer et al., 2014; Song et al., 2020). The EB1-GFP signal with the intensity at 300–800 a.u. and the dwell time within 5 sec were selected as a single molecule (Supplementary Figure S3B). To exclude the influence of different growth rates, we equalized the growth rates of microtubules by using 5 μM α1A/β2A and 2.5 μM α1C/β2A. Under these tubulin concentrations, α1A/β2A microtubules grew at 0.80 ± 0.31 μm/min and α1C/β2A microtubules grew at 0.86 ± 0.30 μm/min in the presence of 5 nM EB1-GFP (Supplementary Figure S3A). Using a previously published method (Maurer et al., 2014; Song et al., 2020), we applied single-molecule tracking and comet averaging to measure the length of EB1 comets. Fitting the averaged comet profiles to a model of EB binding, which resembled the shape of the fluorescence profiles of EB1 comets, showed that the length of GTP cap for α1A/β2A microtubules was similar to that of α1C/β2A microtubules (Figure 5B), suggesting that α1A/β2A and α1C/β2A microtubules have similar GTP hydrolysis rates. Taken together, these data indicate that the lower catastrophe frequency of α1C/β2A microtubules is mainly due to the increase in growth rate rather than changes in GTP hydrolysis rate.

EB1 but not kinesin-1 shows different behaviors on α1C/β2A microtubules compared to α1A/β2A microtubules

Previous study proposes that the C-terminal tail specifies the interaction of tubulin with some MAPs (Sirajuddin et al., 2014), e.g. EB1 (Zanic et al., 2009). Since the microtubules composed of α1A/β2A and α1C/β2A exhibited different polymerization dynamics, and α1A and α1C isotypes had different C-terminal tails, we explored whether MAPs had different binding properties with α1A/β2A and α1C/β2A microtubules using EB1 and kinesin-1 as two examples. First, we used the TIRF-based single-molecule assay to analyze the EB1-binding ability with microtubules, including the on-rate and dwell time of EB1. Under similar growth rates of microtubules (Supplementary Figure S3A), the dwell time of EB1-GFP on the plus-ends of α1C/β2A microtubules was significantly longer

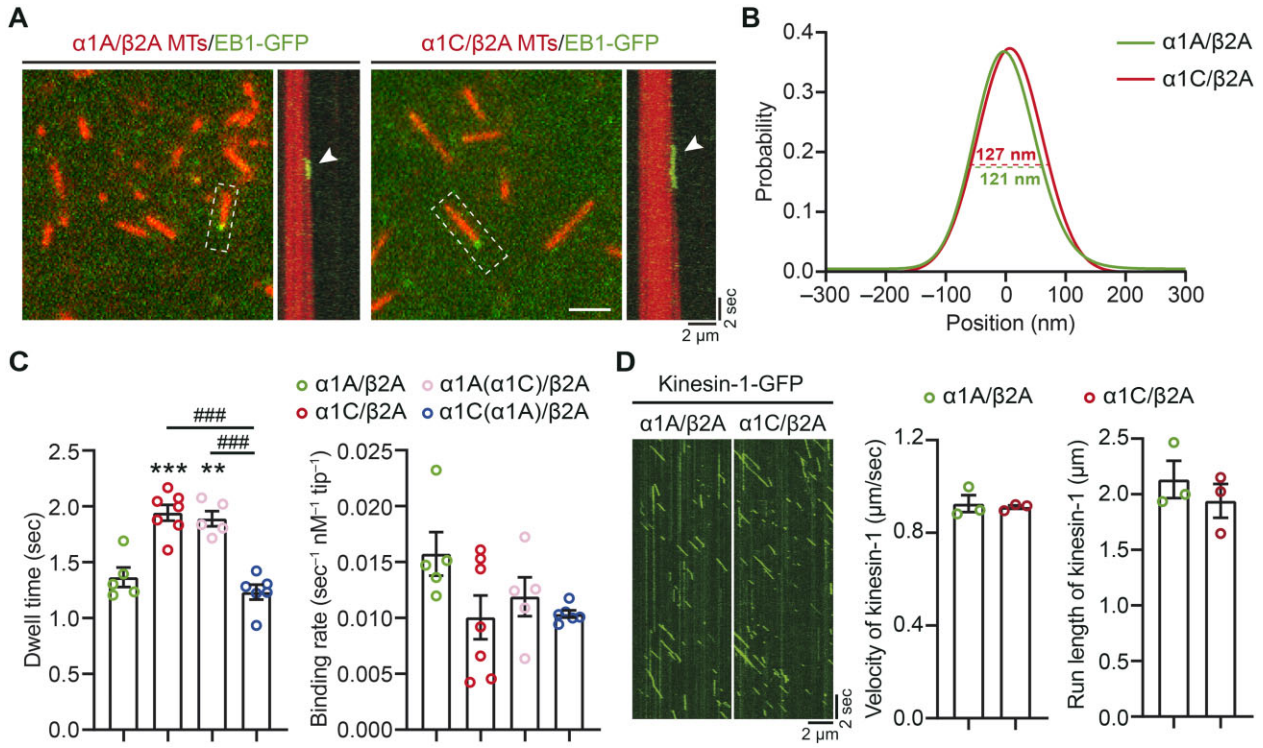

Figure 5 The binding abilities of EB1 and kinesin-1 on α1A/β2A and α1C/β2A microtubules. (**A**) Representative TIRF images and kymographs of single-molecule detection assay for EB1. α1A/β2A and α1C/β2A microtubules mixed with ~4% rhodamine-labeled porcine brain tubulin (red) and EB1-GFP (green) are shown. Scale bar, 2 μm. (**B**) The spatial distribution of EB1-GFP binding events along the longitudinal axis of microtubules in the presence of 5 nM EB1-GFP, fitting to an exponentially modified Gaussian function. The green line shows the spatial distribution of EB1-GFP binding events ($n = 177$) on α1A/β2A microtubule. The red line shows the spatial distribution of EB1-GFP binding events ($n = 226$) on α1C/β2A microtubule. (**C**) Left: histogram showing the dwell time of EB1-GFP on α1A/β2A ($n = 5$, containing 398 events), α1C/β2A ($n = 7$, containing 272 events), α1A(α1C)/β2A ($n = 5$, containing 247 events), and α1C(α1A)/β2A microtubules ($n = 6$, containing 280 events). Right: histogram showing the apparent association rates of EB1-GFP on α1A/β2A ($n = 5$, containing 189 events), α1C/β2A ($n = 7$, containing 106 events), α1A(α1C)/β2A ($n = 5$, containing 105 events), and α1C(α1A)/β2A ($n = 6$, containing 106 events) microtubules. The data are presented as mean ± SEM. $^{**}P < 0.01$, $^{***}P < 0.001$ vs. α1A/β2A microtubules, and $^{\#\#\#}P < 0.001$ vs. indicated; Student's *t*-test. (**D**) Left: kinesin-1 motility on α1A/β2A and α1C/β2A microtubules. Kymographs showing kinesin-1-GFP movement on these microtubules. Right: histograms showing the velocity and run length of kinesin-1-GFP on these microtubules ($n = 3$, α1A/β2A microtubules containing 151 motor measurements and α1C/β2A microtubules containing 155 motor measurements). The data are presented as mean ± SEM; Student's *t*-test.

than that of α1A/β2A microtubules, which was reversed when α1A and α1C exchanged their C-terminal tails (Figure 5C). Meanwhile, the on-rates of EB1-GFP were similar on two types of microtubules (Figure 5C). Altogether, these results suggest that EB1 has a higher binding ability on α1C/β2A microtubules than α1A/β2A microtubules.

Finally, we explored whether molecular motors, e.g. kinesin-1, exhibited different motility on α1A/β2A and α1C/β2A microtubules. Kinesin-1 is a ubiquitously expressed motor that transports vesicles, mitochondria, mRNA, and other cargos (Hirokawa et al., 2009). Using a TIRF-based single-molecule motility assay, we measured the moving velocity and run length of kinesin-1 on α1A/β2A and α1C/β2A microtubules (Figure 5D; Supplementary Figure S2B). Both moving velocity and run length of kinesin-1 were similar between α1A/β2A and α1C/β2A microtubules (Figure 5D). Therefore, α1A and α1C do not exhibit different effects on the motility of kinesin-1.

Discussion

The precisely regulated dynamics of microtubules is important for their versatile cellular functions. Microtubules are composed of α/β-tubulin dimers and vertebrates have multiple tubulin genes. Here, we study the effects of α-tubulin isotypes α1A and α1C on microtubule assembly properties. Microtubules composed of α1A/β2A grow slowly and undergo a higher catastrophe, while α1C/β2A microtubules have a faster growth rate and lower catastrophe and finally result in a longer length, which were mainly caused by their C-terminal tail and plus-end affinity. Additionally, some MAPs show distinct binding properties on these two types of microtubules, i.e. EB1 had

a longer dwell time on α1C/β2A microtubules, but kinesin-1 displayed similar motility on both microtubules. These findings expand our current knowledge of α-tubulin isotypes on microtubule dynamics.

Microtubules are important cytoskeletal polymers that play a variety of essential roles in cells. Previous studies have reported that α/β-tubulin dimers with different composition of β-tubulin isotypes, which were obtained by using antibody-based immuno-affinity chromatography or insect cell-based strategy, displayed distinct microtubule dynamics (Panda et al., 1994; Pamula et al., 2016; Vemu et al., 2017). In the present study, we purified exogenous-expressed α1A/β2A, α1B/β2A, and α1C/β2A from insect cells and performed *in vitro* microtubule reconstitution assay. We detected that α1A/β2A and α1B/β2A microtubules displayed similar dynamics, while α1C/β2A microtubules had a higher growth rate and lower catastrophe frequency, indicating that the microtubule dynamics is also controlled by α-tubulin isotypes. Furthermore, by mixing different ratios of α1A/β2A and α1C/β2A to mimic the situation of multiple tubulin isotypes in cells, we found that the parameters of these mixed microtubules were not simply proportional to the ratios of α1A/β2A and α1C/β2A. A previous study also revealed that the microtubules composed of mixed α/βII and α/βIII were significantly less dynamic than those formed from either α/βII or α/βIII (Panda et al., 1994). Whether the incorporation efficiency of different tubulin isotypes into microtubules is unequivalent or some properties of microtubules are more likely influenced by specific tubulin isotypes needs to be further investigated. Nevertheless, the present study provides evidences supporting a significant effect of α-tubulin isotypes on microtubule dynamics.

Since tubulin isotypes are highly conserved, the C-terminal tails of tubulins are the most variable part. In the present study, we exchanged the C-terminal tails of α1A and α1C with each other and found their microtubule dynamics interchanged, indicating that the specific polymerization properties are mainly controlled by their C-terminal tails, which was not similar to β-tubulin isotypes. Previous study reports that the core structure of β-tubulin confers isotype-specific polymerization properties rather than the diverse C-terminal tails (Pamula et al., 2016). However, exchange of two different amino acids in the core structure between α1A and α1C did not significantly change microtubule dynamics. One exception was that replacement of the serine 232 residue of α1C with the glycine residue of α1A, α1C(S232G)/β2A, resulted in the growth rate and maximum length of α1C/β2A microtubules close to that of α1A/β2A microtubules. Although one of the differential amino acids in the core structure of α1A and α1C contributes a little bit to some parameters of microtubule dynamics, the C-terminal tails of α-tubulin mainly endow isotype-specific polymerization properties.

Microtubule growth rate at plus-ends is sped up with increased tubulin concentrations and can be fitted to a regression line, whose slope (k_{on}) represents the affinity of tubulin dimer for microtubule plus-ends (Oosawa, 1970). In the present study, we found that the growth rate for α1C/β2A microtubules was ~2-fold faster than that for α1A/β2A microtubules, and the k_{on} of α1C/β2A was higher than that of α1A/β2A, suggesting that α1C/β2A has a higher affinity to microtubule plus-ends than α1A/β2A. Consistent with our studies, the faster growing αIB/(βI + βIVB) microtubules had a higher k_{on} than the lower growing microtubules composed of brain tubulin (Vemu et al., 2017), and the faster growing *Caenorhabditis elegans* microtubules also displayed a higher k_{on} than the lower growing microtubules consisted of *Bos taurus* brain tubulin (Chaaban et al., 2018), while the similar growing α/βII and α/βIII microtubules had an equivalent k_{on} (Pamula et al., 2016; Ti et al., 2016). On the other hand, polymerizing microtubules are protected from depolymerization by a GTP cap at their ends. Slower GTP hydrolysis rate confers an instantaneous stability to the polymers (Duellberg et al., 2016). By using the single-molecule detection assay for EB1, we found that the GTP hydrolysis rates of α1A/β2A and α1C/β2A microtubules were similar. Therefore, the faster growth rate and lower catastrophe frequency of α1C/β2A compared to α1A/β2A microtubules are mostly due to the C-terminal tail-determined higher affinity of α1C/β2A at plus-ends but not the GTP hydrolysis rate of microtubules.

Previous studies have shown that the lattice binding of MAPs is mediated by the C-terminal tail of tubulin (Helenius et al., 2006; Brouhard et al., 2008; Cooper and Wordeman, 2009; Zanic et al., 2009). In the present study, α1C/β2A microtubules exhibited a higher EB1-binding affinity than α1A/β2A microtubules, and this phenomenon was reversed by swapping the C-terminal tails of α1A and α1C tubulins. Additionally, the dwell time of EB1 on both α1A/β2A and α1C/β2A microtubules was longer than reported in previous studies, usually <1 sec (Maurer et al., 2014; Song et al., 2020), which was probably caused by the strong electronegative Flag tag at the C-terminal tail of β2A, because EB1 bound the microtubule lattice through an electrostatic interaction with the C-terminal tail of tubulin (Zanic et al., 2009). In contrast, both the velocity and run length of kinesin-1 on α1A/β2A and α1C/β2A microtubules were similar, supporting previous study showing that kinesin-1 mostly requires the C-terminal tail of β-tubulin for full activity (Sirajuddin et al., 2014).

In the present study, we purified recombinant α1A/β2A, α1B/β2A, and α1C/β2A and found that microtubule polymerization properties were not only affected by specific α-tubulin isotypes, which was mainly determined by the variable C-terminal tails, but also modulated by the ratios of diverse α-tubulin isotypes. Future studies with other specific tubulin isotypes and different compositions of tubulin isotypes could provide more information on the intricate roles of various tubulin isotypes. Overall, the present study provides evidence for the 'tubulin code' hypothesis and complements the effect of α-tubulin isotypes on microtubule dynamics.

Materials and methods

Plasmids

The expression constructs for α1A (NM_011653.2), α1B (NM_011654.2), α1C (NM_009448.4), and β2A (NM_009450.2)

were cloned from cDNA of mouse brain tissue into the vector pFastBac Dual. α1A, α1B, and α1C sequences were inserted after the polyhedron promoter, and β2A sequence was inserted after the p10 promoter. For affinity purification, a sequence encoding GGSGG linker and a Flag tag were fused to the 3' end of β2A cDNA sequence. For α1A, α1B, and α1C, a His tag was inserted in the acetylation loop (between I42 and G43) (Sirajuddin et al., 2014). An enhancer L21 (Sano et al., 2002) was added to each of these sequences just before the start codon. EB1-GFP was constructed with a GFP tag and a His tag after the full-length human EB1 (NM_012325), and a sequence encoding a PreScission protease site was inserted between the GFP tag and His tag. The constitutively active rat kinesin-1-GFP (rKin430-GFP) plasmid was a gift to Xin Liang from Jonathon Howard (Yale University) and this construct was originally from Rob Cross (Rogers et al., 2001).

Purification of brain tubulin

Mouse brain tubulin was purified as described previously (Castoldi and Popov, 2003). Briefly, wild-type C57/BL6 mouse (adult, 20–25 g) brains were collected and homogenized in cold depolymerization buffer (50 mM MES, 1 mM $CaCl_2$, pH 6.6). Then, through two cycles of polymerization–depolymerization in high-molarity PIPES buffer (1 M PIPES, 10 mM $MgCl_2$, 20 mM EGTA, pH 6.9), the tubulin supernatant was collected, frozen in liquid nitrogen, and stored at −80°C.

Expression and purification of mouse recombinant tubulin

The Bac-to-Bac system (Life Technologies) was used to generate recombinant baculovirus. To express mouse recombinant tubulin composed of His-tagged α-tubulin isotypes (α1A, α1B, or α1C) and Flag-tagged β2A, SF9 cells (Life Technologies) were grown to 2.0–2.5×10^6 cells/ml in Sf-900™ II SFM (Thermo Fisher 10902088) supplemented with antibiotics including penicillin and streptomycin and infected with P3 or P4 viral stocks. Cells were cultured in suspension at 27°C and harvested at 72 h after infection. The following steps were performed at 4°C. Cells were lysed by sonication in lysis buffer (80 mM PIPES, pH 6.9, 100 mM KCl, 1 mM $MgCl_2$, 1 mM EGTA, 0.1 mM GTP, 0.5 mM ATP, 1 mM PMSF), and the lysate was centrifuged for 30 min at 35000 *g*. The supernatant was then filtered through a 0.45-μm Millex-HV PVDF membrane and loaded on a nickel-nitrilotriacetic acid column (Qiagen) pre-equilibrated with lysis buffer. The column was washed with 30–50 ml wash buffer (lysis buffer supplemented with 25 mM imidazole) and then eluted with elution buffer [1× BRB80 (80 mM PIPES, 1 mM $MgCl_2$, 1 mM EGTA), 300 mM imidazole, 0.1 mM GTP, pH 7.0]. The eluate was diluted with an equal volume of BRB80 buffer supplemented with 0.1 mM GTP, and then mixed with anti-Flag antibody-conjugated resin (Sigma-Aldrich) for 2 h. Flag-tagged tubulin was eluted with BRB80 buffer supplemented with 0.2 mg/ml 3× Flag peptide (APE × BIO A6001). The purified tubulin was concentrated and desalted on an Amicon Ultracel-30 K filter (Millipore, Merck KGaA) with BRB80 and 0.1 mM GTP. Small aliquots of tubulin were frozen in liquid nitrogen and stored at −80°C. Using this protocol, we generally yielded 200–600 μg recombinant isotype-specific tubulin dimers per liter of SF9 cells. Additionally, we also tried to purify mouse recombinant tubulin composed of His-tagged α-tubulin isotypes (α1A, α1B, or α1C) and β2A without Flag tag in the C-terminal tail. However, the yield of purified tubulin with the Flag tag removable plasmid was very low, which was not enough for further tag removal and following experiments. Considering that the main purpose in the present study was to detect the different effects of α-tubulin isotypes, the tubulin heterodimer with the same Flag-tagged β2A was acceptable, although it was not perfect.

The purified recombinant tubulins were run on sodium dodecyl sulfate–polyacrylamide gel electrophoresis gel following Coomassie blue staining. Then, three visible bands between 100 and 250 kDa besides tubulin bands were excised and further analyzed by mass spectrometry. The analysis from mass spectrometry showed that the top five contaminated proteins of α1A/β2A and α1C/β2A were the same and represented >90% of the total, including SFRICE_00452, SFRICE_019683, ubiquitin C-terminal hydrolase 7, SFRICE_000333, and SFRICE_022541. The functions of these proteins were not reported to be directly related to microtubule or unknown. The data of mass spectrometry are provided in Supplementary Tables S1 and S2.

Purification of MAPs

The kinesin-1-GFP and EB1-GFP were expressed and purified from *Escherichia coli* BL21(DE3) using a protocol that was modified from the previously published methods (Maurer et al., 2011; Tas et al., 2017). The transformed *E.coli* BL21(DE3) cells were cultured in Luria–Bertani medium (LB) at 20°C and collected at 16 h after induction with 0.5 mM isopropyl 1-thio-b-galactopyranoside (Sigma). Cells were lysed by sonication in lysis buffer (20 mM PIPES, pH 6.9, 150 mM KCl, 4 mM $MgCl_2$, 0.1 mM ATP, 1 mM PMSF). The lysate was cleared by centrifugation at 35000 *g* for 20 min at 4°C. The supernatant was filtered through a 0.45-μm filter and loaded on a nickel-nitrilotriacetic acid column (Qiagen) pre-equilibrated with lysis buffer. The column was washed with 30–50 ml wash buffer and eluted with elution buffer (80 mM PIPES, pH 6.9, 4 mM $MgCl_2$, 1 mM EGTA, 300 mM imidazole, 0.1 mM ATP). The proteins were concentrated and gel-filtrated on a Superdex™ 75 10/300 GL size exclusion chromatography column (GE Healthcare) equilibrated with stock buffer (80 mM PIPES, pH 6.9, 100 mM KCl, 4 mM $MgCl_2$, 1 mM EGTA, 0.1 mM ATP). Protein fractions containing the target protein were collected and concentrated. The protein concentration was estimated by UV at 280 nm, frozen in liquid nitrogen, and stored at −80°C. For EB1-GFP, the crude protein was mixed with a final concentration of 4 U PreScission protease (Beyotime) before size exclusion

chromatography and incubated at 4°C overnight to remove the His tag, and the buffer used to purify EB1-GFP did not require ATP.

Preparation of GMPCPP-stabilized microtubules for Cryo-EM

For the construction of GMPCPP-stabilized α1A/β2A and α1C/β2A microtubules, 15–20 μM α1A/β2A or α1C/β2A tubulins were incubated with 1 mM GMPCPP (Jena Biosciences) at 37°C for 1 h. To remove unpolymerized tubulin, the solution was centrifuged at 126000 *g* for 5 min at 27°C and the supernatant was discarded. Then, the microtubule pellet was resuspended in cold BRB80 and depolymerized at 4°C for 20 min, followed by a second round of polymerization at 37°C with 1 mM GMPCPP for 1 h. Microtubule seeds were pelleted as above and resuspended in 37°C pre-warmed BRB80 with ∼80% volume of initial reaction. The microtubule solution was diluted at a ratio of 1:2–1:3, and 2.2 μl was applied to the plasma-cleaned grid using a Vitrobot Mark IV (Thermo Fisher Scientific). Images were collected using a Titan Krios transmission electron microscope (Thermo Fisher Scientific) operated at 300 kV. All images were recorded on a K2 Summit direct electron detector (Gatan) at a nominal magnification of 18000×, yielding a pixel size of 1.3 Å.

In vitro microtubule reconstitution assay

In vitro microtubule reconstitution and imaging for dynamic growth of mouse recombinant tubulin were performed according to the previous report (Gell et al., 2010). Mouse recombinant tubulin was mixed with HiLyte-488-labeled brain tubulin (Cytoskeleton), grew from rhodamine-labeled GMPCPP-stabilized microtubule seeds, and imaged by TIRF microscopy.

For the construction of rhodamine-labeled or Alexa-647-labeled and GMPCPP-stabilized brain microtubule seeds, we used a similar method as the preparation of GMPCPP-stabilized microtubules for Cryo-EM. For the GMPCPP-stabilized microtubule seeds, tubulins were composed of 80% unlabeled mouse brain tubulin, 10% biotin-tubulin (Cytoskeleton), and 10% rhodamine-tubulin (Cytoskeleton) or Alexa-647-tubulin (Cytoskeleton). The microtubule seeds were frozen in liquid nitrogen and stored at −80°C. The GMPCPP-stabilized microtubule seeds were immobilized onto neutravidin-coated glass.

The sample chamber was prepared by cleaning and silanizing the 18 mm × 18 mm glass coverslips. The flow chamber was assembled from the glass coverslips onto microscopic slides with a double-sided tape. The imaging reaction buffer consisted of 1× BRB80 supplemented with 25 mM glucose, 300 μM glucose oxidase, 100 μM catalase, 0.25 mg/ml bovine serum albumin (BSA), 75 mM KCl, 5 mM dithiothreitol, 0.1% methylcellulose, and 1 mM GTP. The sample was sealed with nail polish. During the experiment, the sample was kept at 37°C ± 1°C. Imaging was started 5 min after placing the chamber on a temperature-controlled workstation (37°C ± 1°C) with the microscope. The dynamic growth of microtubules was imaged at 3-sec intervals for 15 min via TIRF microscopy with Zeiss cell observer spinning disk system and a 100× oil lens. The images were recorded with a pixel size of 160 nm.

Analysis of microtubule dynamics

The kymographs were generated using ImageJ 2.0 software (NIH) and further analyzed with the Image-Pro Plus 5.1 software (Media Cybernetics). The parameters of microtubule dynamic instability were determined from a kymograph. The growth rate of microtubules was calculated as the average rate of either individual growth episode from start of growth to catastrophe. The catastrophe frequency was calculated as the number of events per total time of microtubule growth. The maximum length of microtubules was calculated as the longest distance of each microtubule during its growth episode.

Single-molecule assay

For EB1, during *in vitro* microtubule reconstitution, 5 nM EB1-GFP was added with different tubulin isotypes to the reaction buffer containing 1× BRB80, 25 mM glucose, 300 nM glucose oxidase, 100 nM catalase, 0.25 mg/ml BSA, 75 mM KCl, 2 mM $MgCl_2$, 5 mM dithiothreitol, and 1 mM GTP. In this assay, the dynamic microtubule and EB1-GFP single molecule were recorded using a TIRF microscope (Olympus) equipped with an Andor 897 Ultra EMCCD camera (Andor) using a 100× TIRF objective (NA 1.49; Olympus). Alexa-647-labeled microtubule seeds were used and time-lapse TIRF imaging was acquired at 0.1-sec intervals with a 0.05-sec exposure for 5 min at 37°C. Microtubule end tracking and further analysis were performed according to previous description (Maurer et al., 2014; Song et al., 2020). Briefly, rhodamine-labeled microtubule plus-ends were automatically tracked by a MATLAB program (MathWorks). A two-dimensional model describing the microtubule lattice as a Gaussian wall and the microtubule plus-end as a half-Gaussian was fitted to the area in the original image where microtubules were identified, which was used to locate the plus-ends of microtubules at each frame. Then, the position of microtubule ends was used as a reference in aligning and averaging the EB1-GFP comet signals in the time-lapse images. To measure the position of individual EB1-GFP molecules at microtubule ends, a Gaussian function was used to fit the intensity profile of individual EB1-GFP molecules. The peak location (relative to the position of the microtubule end) was recorded as the position of each EB1-GFP. The positional distribution of EB1-GFP binding sites was plotted along the longitudinal axis of microtubules and fitted to an exponentially modified Gaussian function to calculate the full width at half maximum as an estimation of the length of the EB1-binding region.

For kinesin-1, GMPCPP-stabilized α1A/β2A or α1C/β2A microtubules containing 5% rhodamine-tubulin and 5% biotin-tubulin were seeded into the chamber. Then, the imaging buffer containing 1× BRB80, 1 nM kinesin-1-GFP, 25 mM glucose, 300 nM glucose oxidase, 100 nM catalase, 0.25 mg/ml BSA, and 1.5 mM ATP was added into the chamber. Time-lapse TIRF

imaging was acquired at 0.1-sec intervals for 2 min at 37°C. The images were recorded with a pixel size of 80 nm. The velocity and run length of kinesin-1 were calculated using the kymograph analysis in ImageJ software.

Statistical analysis

Data were acquired from at least three independent experiments and presented as mean ± SEM. Statistical significance was analyzed using Student's unpaired *t*-test using Prism 8 software (GraphPad). The measurements of k_{on} and k_{off} were performed in OriginLab software using linear fitting weighted with the standard deviation. Differences were considered significant at the level of $P < 0.05$.

Supplementary material

Supplementary material is available at *Journal of Molecular Cell Biology* online.

Acknowledgements

We thank the Integrated Laser Microscopy System at National Facility for Protein Science in Shanghai (NFPS), Zhangjiang Lab, China for their technical assistance. We also thank Shifei Wu, Yue Yin, and Dr Chao Peng of the Mass Spectrometry System at NFPS for data collection and analysis.

Funding

This work was supported by grants from the National Natural Science Foundation of China (31991194, 31330046, and 31922018) and the Strategic Priority Research Program of Chinese Academy of Sciences (XDB19000000).

Conflict of interest: none declared.

Author contributions: L.D. did most experiments. M.-Y.L. helped with the protein purification and detection of microtubule dynamics. Y.-L.S. helped with *in vitro* EB1 imaging supervised by X.L. X.Z. helped with the experiment design. L.D. and L.B. wrote the manuscript. X.L. helped with manuscript revision. L.B. supervised the whole project.

References

Albahde, M.A.H., Zhang, P., Zhang, Q., et al. (2020). Upregulated expression of TUBA1C predicts poor prognosis and promotes oncogenesis in pancreatic ductal adenocarcinoma via regulating the cell cycle. Front. Oncol. *10*, 49.

Bahi-Buisson, N., Poirier, K., Fourniol, F., et al. (2014). The wide spectrum of tubulinopathies: what are the key features for the diagnosis? Brain *137*, 1676–1700.

Bamji, S.X., and Miller, F.D. (1996). Comparison of the expression of a Tα1: nlacZ transgene and Tα1 α-tubulin mRNA in the mature central nervous system. J. Comp. Neurol. *374*, 52–69.

Banerjee, A., Roach, M.C., Wall, K.A., et al. (1988). A monoclonal antibody against the type II isotype of β-tubulin. Preparation of isotypically altered tubulin. J. Biol. Chem. *263*, 3029–3034.

Bian, T., Zheng, M., Jiang, D., et al. (2021). Prognostic biomarker TUBA1C is correlated to immune cell infiltration in the tumor microenvironment of lung adenocarcinoma. Cancer Cell Int. *21*, 144.

Bowne-Anderson, H., Zanic, M., Kauer, M., et al. (2013). Microtubule dynamic instability: a new model with coupled GTP hydrolysis and multistep catastrophe. Bioessays *35*, 452–461.

Breuss, M., and Keays, D.A. (2014). Microtubules and neurodevelopmental disease: the movers and the makers. Adv. Exp. Med. Biol. *800*, 75–96.

Brouhard, G.J., Stear, J.H., Noetzel, T.L., et al. (2008). XMAP215 is a processive microtubule polymerase. Cell *132*, 79–88.

Castoldi, M., and Popov, A.V. (2003). Purification of brain tubulin through two cycles of polymerization-depolymerization in a high-molarity buffer. Protein Expr. Purif. *32*, 83–88.

Chaaban, S., Jariwala, S., Hsu, C.T., et al. (2018). The structure and dynamics of C. elegans tubulin reveals the mechanistic basis of microtubule growth. Dev. Cell *47*, 191–204.

Chakraborti, S., Natarajan, K., Curiel, J., et al. (2016). The emerging role of the tubulin code: from the tubulin molecule to neuronal function and disease. Cytoskeleton *73*, 521–550.

Cooper, J.R., and Wordeman, L. (2009). The diffusive interaction of microtubule binding proteins. Curr. Opin. Cell Biol. *21*, 68–73.

Duellberg, C., Cade, N.I., Holmes, D., et al. (2016). The size of the EB cap determines instantaneous microtubule stability. eLife *5*, e13470.

Fackenthal, J.D., Turner, F.R., and Raff, E.C. (1993). Tissue-specific microtubule functions in Drosophila spermatogenesis require the β2-tubulin isotype-specific carboxy terminus. Dev. Biol. *158*, 213–227.

Gell, C., Bormuth, V., Brouhard, G.J., et al. (2010). Microtubule dynamics reconstituted in vitro and imaged by single-molecule fluorescence microscopy. Methods Cell Biol. *95*, 221–245.

Gloster, A., El-Bizri, H., Bamji, S.X., et al. (1999). Early induction of Tα1 α-tubulin transcription in neurons of the developing nervous system. J. Comp. Neurol. *405*, 45–60.

Heald, R., and Khodjakov, A. (2015). Thirty years of search and capture: the complex simplicity of mitotic spindle assembly. J. Cell Biol. *211*, 1103–1111.

Helenius, J., Brouhard, G., Kalaidzidis, Y., et al. (2006). The depolymerizing kinesin MCAK uses lattice diffusion to rapidly target microtubule ends. Nature *441*, 115–119.

Hirokawa, N., Noda, Y., Tanaka, Y., et al. (2009). Kinesin superfamily motor proteins and intracellular transport. Nat. Rev. Mol. Cell Biol. *10*, 682–696.

Hoyle, H.D., and Raff, E.C. (1990). Two Drosophila β tubulin isoforms are not functionally equivalent. J. Cell Biol. *111*, 1009–1026.

Jiang, Y.Q., and Oblinger, M.M. (1992). Differential regulation of βIII and other tubulin genes during peripheral and central neuron development. J. Cell Sci. *103*, 643–651.

Keays, D.A., Tian, G., Poirier, K., et al. (2007). Mutations in α-tubulin cause abnormal neuronal migration in mice and lissencephaly in humans. Cell *128*, 45–57.

Lecine, P., Italiano, J.E., Jr., Kim, S.W., et al. (2000). Hematopoietic-specific β1 tubulin participates in a pathway of platelet biogenesis dependent on the transcription factor NF-E2. Blood *96*, 1366–1373.

Maurer, S.P., Bieling, P., Cope, J., et al. (2011). GTPγS microtubules mimic the growing microtubule end structure recognized by end-binding proteins (EBs). Proc. Natl Acad. Sci. USA *108*, 3988–3993.

Maurer, S.P., Cade, N.I., Bohner, G., et al. (2014). EB1 accelerates two conformational transitions important for microtubule maturation and dynamics. Curr. Biol. *24*, 372–384.

Minoura, I., Hachikubo, Y., Yamakita, Y., et al. (2013). Overexpression, purification, and functional analysis of recombinant human tubulin dimer. FEBS Lett. *587*, 3450–3455.

Mitchison, T., and Kirschner, M. (1984). Dynamic instability of microtubule growth. Nature *312*, 237–242.

Neff, N.F., Thomas, J.H., Grisafi, P., et al. (1983). Isolation of the β-tubulin gene from yeast and demonstration of its essential function in vivo. Cell *33*, 211–219.

Oosawa, F. (1970). Size distribution of protein polymers. J. Theor. Biol. *27*, 69–86.

Pamula, M.C., Ti, S.C., and Kapoor, T.M. (2016). The structured core of human β tubulin confers isotype-specific polymerization properties. J. Cell Biol. *213*, 425–433.

Panda, D., Miller, H.P., Banerjee, A., et al. (1994). Microtubule dynamics in vitro are regulated by the tubulin isotype composition. Proc. Natl Acad. Sci. USA *91*, 11358–11362.

Rogers, K.R., Weiss, S., Crevel, I., et al. (2001). KIF1D is a fast non-processive kinesin that demonstrates novel K-loop-dependent mechanochemistry. EMBO J. *20*, 5101–5113.

Saillour, Y., Broix, L., Bruel-Jungerman, E., et al. (2014). Beta tubulin isoforms are not interchangeable for rescuing impaired radial migration due to Tubb3 knockdown. Hum. Mol. Genet. *23*, 1516–1526.

Sano, K., Maeda, K., Oki, M., et al. (2002). Enhancement of protein expression in insect cells by a lobster tropomyosin cDNA leader sequence. FEBS Lett. *532*, 143–146.

Schatz, P.J., Pillus, L., Grisafi, P., et al. (1986). Two functional α-tubulin genes of the yeast Saccharomyces cerevisiae encode divergent proteins. Mol. Cell. Biol. *6*, 3711–3721.

Sirajuddin, M., Rice, L.M., and Vale, R.D. (2014). Regulation of microtubule motors by tubulin isotypes and post-translational modifications. Nat. Cell Biol. *16*, 335–344.

Song, Y., Zhang, Y., Pan, Y., et al. (2020). The microtubule end-binding affinity of EB1 is enhanced by a dimeric organization that is susceptible to phosphorylation. J. Cell Sci. *133*, jcs241216.

Tas, R.P., Chazeau, A., Cloin, B.M.C., et al. (2017). Differentiation between oppositely oriented microtubules controls polarized neuronal transport. Neuron *96*, 1264–1271.

Theurkauf, W.E., Baum, H., Bo, J., et al. (1986). Tissue-specific and constitutive α-tubulin genes of Drosophila melanogaster code for structurally distinct proteins. Proc. Natl Acad. Sci. USA *83*, 8477–8481.

Ti, S.C., Pamula, M.C., Howes, S.C., et al. (2016). Mutations in human tubulin proximal to the kinesin-binding site alter dynamic instability at microtubule plus- and minus-ends. Dev. Cell *37*, 72–84.

Ti, S.C., Wieczorek, M., and Kapoor, T.M. (2020). Purification of affinity tag-free recombinant tubulin from insect cells. STAR Protocols *1*, 100011.

Vemu, A., Atherton, J., Spector, J.O., et al. (2016). Structure and dynamics of single-isoform recombinant neuronal human tubulin. J. Biol. Chem. *291*, 12907–12915.

Vemu, A., Atherton, J., Spector, J.O., et al. (2017). Tubulin isoform composition tunes microtubule dynamics. Mol. Biol. Cell *28*, 3564–3572.

Wang, J., Chen, W., Wei, W., et al. (2017). Oncogene TUBA1C promotes migration and proliferation in hepatocellular carcinoma and predicts a poor prognosis. Oncotarget *8*, 96215–96224.

Zanic, M., Stear, J.H., Hyman, A.A., et al. (2009). EB1 recognizes the nucleotide state of tubulin in the microtubule lattice. PLoS One *4*, e7585.